



# Structure of RavA MoxR AAA+ protein reveals the design principles of a molecular cage modulating the inducible lysine decarboxylase activity

Majida El Bakkouri<sup>a</sup>, Irina Gutsche<sup>b</sup>, Usheer Kanjee<sup>a</sup>, Boyu Zhao<sup>a</sup>, Miao Yu<sup>a</sup>, Gael Goret<sup>c</sup>, Guy Schoehn<sup>b,c</sup>, Wim P. Burmeister<sup>b,d</sup>, and Walid A. Houry<sup>a,1</sup>

<sup>a</sup>Department of Biochemistry, University of Toronto, Toronto, ON, Canada M5S 1A8; <sup>b</sup>Unit for Virus Host-Cell Interactions (UVHCI), Unité Mixte de Internationale (UMI) 3265, Université Joseph Fourier (UJF)-European Molecular Biology Laboratory (EMBL) Grenoble Outstation-Centre National de la Recherche Scientifique (CNRS), 6 rue Jules Horowitz, 38042 Grenoble, France; <sup>c</sup>Institut de Biologie Structurale (IBS) Jean-Pierre Ebel, Unité Mixte de Recherche (UMR) 5075, Commissariat à l'Énergie Atomique (CEA)-CNRS-UJF, 41 rue Jules Horowitz, 38027 Grenoble, France; and <sup>d</sup>Institut Universitaire de France (IUF), 103 Boulevard St. Michel, 75005 Paris, France

Edited by Gregory A. Petsko, Brandeis University, Waltham, MA, and approved November 5, 2010 (received for review June 24, 2010)

The MoxR family of AAA+ ATPases is widespread throughout bacteria and archaea but remains poorly characterized. We recently found that the *Escherichia coli* MoxR protein, RavA (Regulatory ATPase variant Δ), tightly interacts with the inducible lysine decarboxylase, LdcI/CadA, to form a unique cage-like structure. Here, we present the X-ray structure of RavA and show that the  $\alpha\beta\alpha$  and all- $\alpha$  subdomains in the RavA AAA+ module are arranged as in magnesium chelatases rather than as in classical AAA+ proteins. RavA structure also contains a discontinuous triple-helical domain as well as a  $\beta$ -barrel-like domain forming a unique fold, which we termed the LARA domain. The LARA domain was found to mediate the interaction between RavA and LdcI. The RavA structure provides insights into how five RavA hexamers interact with two LdcI decamers to form the RavA-LdcI cage-like structure.

acid stress | alarmone

Proteins of the AAA+ superfamily (ATPases Associated with diverse cellular Activities) are highly ubiquitous and found in all kingdoms of life. These proteins are characterized by the structural conservation of a central ATPase domain of about 250 amino acids called the AAA+ module (1, 2). AAA+ ATPases employ the energy derived from ATP hydrolysis to remodel proteins, DNA, or RNA. Typically, the AAA+ domain can be divided into two structural subdomains, an N-terminal P-loop NTPase  $\alpha\beta\alpha$  subdomain that is connected to a smaller C-terminal all- $\alpha$  subdomain. The  $\alpha\beta\alpha$  subdomain adopts a Rossman fold and contains several motifs involved in ATP binding and hydrolysis, including Walker A, Walker B, and Sensor 1 signature sequences (3–6). The all- $\alpha$  subdomain, which contains the Sensor 2 motif (7), is much less conserved across AAA+ proteins.

AAA+ proteins form oligomers, usually hexameric rings, in the presence of nucleotides (8). The ATP-binding pocket is located at the interface between two neighboring subunits. A highly conserved arginine from one subunit, called an “arginine finger,” contacts the  $\gamma$ -phosphate of bound ATP of the neighboring subunit (9). AAA+ proteins typically go through a cycle of ATP binding, hydrolysis, and release of products. This reaction cycle results in a series of conformational changes and mechanical movements that allow these proteins to exert their activity either directly or through domains attached to the AAA+ domain (3, 10).

The RavA protein (Regulatory ATPase Variant Δ) belongs to the MoxR AAA+ family (11). Limited experimental data suggest a function of MoxR AAA+ proteins as chaperones in the assembly of multimeric complexes and a possible role in small molecule cofactor insertion/removal (11). However, how these proteins act is not clear. In *Escherichia coli*, the *ravA* gene is in an operon with another gene of unknown function, which we termed *viaA*, and the operon is under the control of  $\sigma^S$  promoter, suggesting a function of RavA and ViaA under stress conditions (12). This is

further substantiated by our discovery that RavA physically interacts with the inducible lysine decarboxylase enzyme, LdcI/CadA, a key enzyme in the bacterial acid stress response. We have visualized the LdcI-RavA complex by negative staining electron microscopy and found it to form a large, about 3.3 MDa, unusual cage-like structure consisting of two LdcI decamers that are linked by up to five RavA hexamers (12). Because LdcI is fivefold symmetric whereas RavA is sixfold symmetric, understanding the construction of this complex is important to understanding how the symmetry mismatch was used in forming the cage-like structure.

We recently solved the X-ray crystal structure of LdcI decamer and unexpectedly found that LdcI activity is strongly inhibited by the binding of the alarmone, ppGpp (further details on the LdcI structure will be described elsewhere). Here, we have determined the three-dimensional structure of RavA full-length protein as a monomer in complex with ADP by X-ray crystallography. Insights into the intersubunit organization of the hexameric RavA were obtained from electron microscopy. These structures provided important insights into how nature solved the symmetry mismatch problem between the fivefold symmetric LdcI decamer and sixfold symmetric RavA hexamer to allow for the construction of the RavA-LdcI molecular cage-like structure. We show that the RavA-LdcI interaction reduces the inhibition of LdcI activity by the alarmone ppGpp in vitro as well as in vivo. The biological implications of this interaction are discussed.

## Results

**The Overall Structure of RavA Protomer.** RavA full-length recombinant protein was expressed and purified to homogeneity as previously described (12). Purity was tested by mass spectrometry and light scattering. RavA crystals were obtained several years ago but failed to diffract to better than 7 Å resolution. High-quality crystals were finally obtained by employing a dehydration protocol as described in *Materials and Methods*. The protein crystallized in the space group  $P6_5$  with one molecule in the asymmetric unit. The crystal structure was solved to 2.9 Å resolution. The model includes 475 of the 498 residues of RavA and one bound ADP molecule, but no electron density corresponding to a Mg<sup>2+</sup> ion was found (Table S1). Two segments, 88–97 and

BIOCHEMISTRY

Author contributions: M.E.B., I.G., U.K., G.S., W.P.B., and W.A.H. designed research; M.E.B., I.G., U.K., B.Z., M.Y., and W.A.H. performed research; M.E.B., I.G., U.K., B.Z., G.G., and W.A.H. analyzed data; and M.E.B., I.G., U.K., B.Z., and W.A.H. wrote the paper.

The authors declare no conflict of interest.

This article is a PNAS Direct Submission.

Data deposition: The crystallography, atomic coordinates, and structure factors have been deposited in the Protein Data Bank, [www.pdb.org](http://www.pdb.org) (PDB ID code 3NBX).

<sup>1</sup>To whom correspondence should be addressed. E-mail: walid.houry@utoronto.ca.

This article contains supporting information online at [www.pnas.org/lookup/suppl/doi:10.1073/pnas.1009092107/DCSupplemental](http://www.pnas.org/lookup/suppl/doi:10.1073/pnas.1009092107/DCSupplemental).

438–441 (Fig. 1A), are missing in the final electron density map and are indicated by dotted lines in Fig. 1B.

The RavA monomer has a complex elongated overall structure consisting of three distinct domains (Fig. 1A and B). The N-terminal domain of RavA is the AAA+ module, which is composed of two subdomains: the  $\alpha\beta\alpha$  subdomain (residues 1–192, brown) and the all- $\alpha$  subdomain (residues 226–306, wheat). The  $\alpha\beta\alpha$  subdomain exhibits a Rossmann-type fold commonly found in nucleotide binding proteins. It consists of a central  $\beta$ -sheet with five parallel  $\beta$ -strands, ordered as 51432, sandwiched between seven  $\alpha$ -helices. The all- $\alpha$  subdomain consists of four antiparallel  $\alpha$ -helices. The  $\alpha\beta\alpha$  subdomain and the all- $\alpha$  subdomain are linked by a 32-residue helical segment (residues 193–225, green). The relative arrangement of the subdomains is similar to that found in Mg chelatases (discussed below).

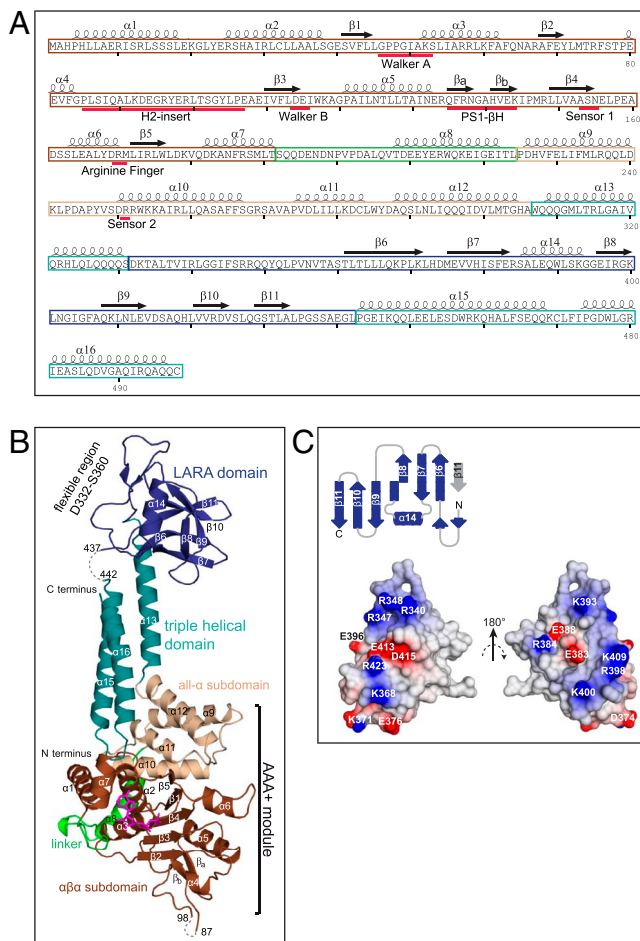


**Fig. 1.** Overall view of RavA protomer structure. (A) Sequence of *E. coli* RavA showing secondary structure and conserved motifs. (B) X-ray structure of RavA protomer.  $\alpha\beta\alpha$  subdomain is shown in brown, all- $\alpha$  subdomain is shown in wheat, the linker between the two subdomains is shown in green, triple-helical bundle domain is shown in blue, the LARA domain is shown in dark blue, and bound ADP is shown in violet. The  $\alpha$ -helices and  $\beta$ -strands are labeled sequentially except for  $\beta_a$  and  $\beta_b$  of the Pre-Sensor 1  $\beta$ -Hairpin insertion. Residues 88–97 and 438–441 were not observed in the X-ray structure and are indicated by a dashed line. The figure was generated using PYMOL. (C) Shown is a topological diagram of the LARA domain drawn using Top-Draw (25) and its electrostatic surface potential calculated using Delphi (26). Colors are according to the calculated electrostatic surface potential and range from red (potential of  $-5$  kT) to blue ( $+5$  kT). The hydrophobic core of the domain is made by the side chains of hydrophobic residues from each of the  $\beta$ -strands ( $\beta$ 1: L362, L364, L366, L372;  $\beta$ 2: V377, I380, F382;  $\beta$ 3: I397, L401;  $\beta$ 4: L410, L412;  $\beta$ 5: L420, V422;  $\beta$ 6: L432) as well as residues L387, W390 and L391 from the  $\alpha$ 14 helix.

The second domain is a discontinuous triple-helical domain formed by helices  $\alpha$ 13,  $\alpha$ 15, and  $\alpha$ 16 (residues 307–330 and 442–497, light blue). This domain has a rigid structure stabilized by hydrophobic interactions localized at the interface between the three helices. The third domain (residues 331–437, dark blue), which we have named the LARA domain (for reasons described below), is a protuberance between helices  $\alpha$ 13 and  $\alpha$ 15 of the triple-helical domain. As shown in Fig. 1B and C, the LARA domain forms a compact antiparallel  $\beta$ -barrel-like structure consisting of six  $\beta$ -strands ( $\beta$ 6– $\beta$ 11) and one  $\alpha$ -helix ( $\alpha$ 14). The LARA domain also includes an N-terminal flexible region (residues D332–S360). The domain is very basic (pI of 9.6) resulting from a highly positively charged surface formed by residues R340, R347, R348, R398, K400, K409, and R423 (Fig. 1C). We performed an extensive search for structures similar to that of the LARA domain in the Protein Data Bank using secondary-structure matching (SSM) (13) and Dali (14), but no such structures were found. Hence, we conclude that the *E. coli* RavA LARA domain adopts a unique fold.

The sequence conservation at the C terminus of RavA spanning the triple-helical and LARA domains diverges quite quickly, although, according to secondary-structure prediction, all organisms containing RavA protein with a LARA domain also have a triple-helical domain. It was surprising to find that a phenylalanine (F472), located at the turn between helices  $\alpha$ 15 and  $\alpha$ 16 of the triple-helical domain, is absolutely conserved (Fig. S1A). This phenylalanine makes hydrophobic contacts with the AAA+ module and, hence, anchors the triple-helical bundle to the AAA+ module (Fig. S1B and C). F472 might serve to transmit the nucleotide-dependent conformational changes in the AAA+ domain to the C-terminal triple-helical and LARA domains of RavA.

**RavA Hexameric Assembly.** Although RavA and many other AAA+ ATPases crystallize as monomers, their functional form is well known to be an oligomeric ring structure. Previous work in our laboratory provided first evidence for a hexameric assembly of RavA induced by ATP, ADP, or 5'-adenylyl- $\beta,\gamma$ -imidodiphosphate (AMPPNP) binding (12). Here we present a 3D structure of the RavA hexamer formed in the presence of ADP obtained by negative staining electron microscopy (EM) and image analysis.

Similar to other AAA+ protein structures, hexameric RavA-ADP is characterized by a ring-shaped core surrounding a central pore. Some representative class averages, as well as corresponding projections of the 3D structure at similar orientations, are shown in Fig. 2A. The distinctive feature of the class averages is the relatively weak density of the LARA domain, which necessitated a good alignment in order to be properly visualized (see Materials and Methods for details). The RavA hexameric ring forms a rather unique flower-like structure and is found to be about 220 Å in diameter and of 80-Å thickness, whereas the diameter of the central channel is about 25 Å. The 3D reconstruction possesses a prominent handedness, visible in the core AAA+ part and notably accentuated by the protrusions. An atomic model of the hexamer was then generated by docking the crystal structure of the monomer into the EM density of the hexamer and adjustment of the resulting intersubunit contacts based on a homology model generated from the hexameric crystal structure of HsIU [PDB ID code 1DOO (15)] (see Materials and Methods and Fig. S2 for details). The final EM reconstruction and the resulting atomic model of the RavA-ADP hexamer are shown in Fig. 2B.

**The Organization of the AAA+ Motor Subdomains.** In their classification of AAA+ proteins, Aravind and coworkers grouped RavA within the helix 2 insert clade (8). Members of this family are found to have (i) an insert within helix 2 of the conserved ASCE (refers to Additional Strand, Catalytic E) division P-loop ATPase core, (ii) a  $\beta$ -hairpin N terminal to Sensor 1, as well as, (iii) a long helical seg-

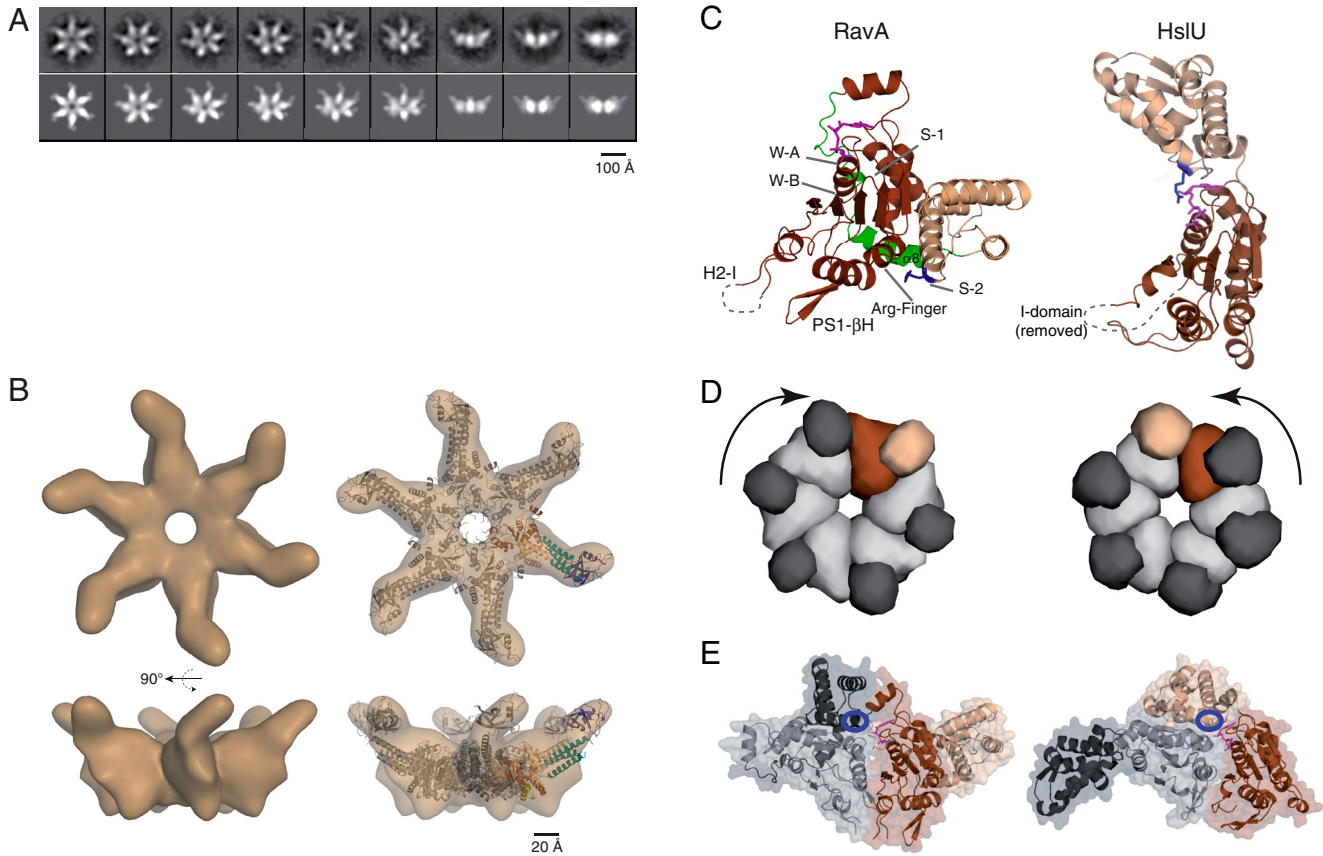


**Fig. 2.** RavA-ADP hexamer structure (*A*, Top) Characteristic class averages of the negatively stained RavA-ADP hexamer; (*B*, Bottom) projections of the final 3D reconstruction at similar orientations. (*B*) Top and side views of the EM 3D reconstruction of the RavA-ADP hexamer. An atomic model of RavA hexamer was generated from the X-ray structure of the RavA protomer by docking into the EM envelope of the hexamer and comparison with the X-ray structure of the HslU hexamer (PDB ID code 1DOO). (*C*) Ribbon representation of RavA AAA+ module (*Left*) and HslU AAA+ module (*Right*, PDB ID code 1DOO). Different subdomains are colored as in Fig. 1 and conserved motifs are shown; the Sensor 2 motif is colored in dark blue and the nucleotide is shown in violet. The I-domain of HslU has been omitted for clarity. (*D*, Left) Schematic representation of RavA AAA+ domain from the hexameric model viewed along the sixfold axis. (*Right*) X-ray structure of HslU hexamer AAA+ domain. For each structure, the  $\alpha\beta\alpha$  and all- $\alpha$  subdomains of one protomer are colored in brown and wheat, respectively. The other protomers are colored in light and dark gray for the  $\alpha\beta\alpha$  and all- $\alpha$  subdomains, respectively. (*E*) Space-filling and ribbon models of a representative dimer of each hexamer in *D*. Nucleotide is shown in violet, whereas the blue circle indicates the location of the Sensor 2 motif.

ment separating the C terminus of the  $\alpha\beta\alpha$  subdomain and the N terminus of the all- $\alpha$  subdomain. The X-ray structure of the RavA AAA+ module agrees with this classification. The  $\alpha\beta\alpha$  subdomain contains two characteristic  $\beta$ -hairpin insertions (Figs. 1*A* and 2*C*). The helix-2 insert (H2-I, residues Pro85–Pro106) is incorporated within helix  $\alpha$ 4, but is partially unstructured in our model (shown as a dotted line in Figs. 1*B* and 2*C*). In the case of the Mg chelatase subunit BchI, this insert consists of two  $\beta$ -strands flanking a small helix (16). The Pre-Sensor 1  $\beta$ -Hairpin insertion (PS1- $\beta$ H, residues Gln135–Pro146) is incorporated between the Sensor 1 strand ( $\beta$ 4) and the preceding helix ( $\alpha$ 5). It has been shown that PS1- $\beta$ H and H2-I are usually important for substrate interaction (17–20). The long helical segment between the  $\alpha\beta\alpha$  and all- $\alpha$  subdomains is shown in green in Figs. 1*A* and *B* and 2*C*; this segment consists of two helices that wrap around the surface of the  $\alpha\beta\alpha$  subdomain making several contacts with it.

SSM and Dali structural similarity searches using the whole RavA AAA+ module indicated only four proteins to have similar structures as the RavA AAA+ domain: the putative ATPase from *Cytophaga hutchinsonii*, BchI subunit of *Rhodobacter capsulatus* Mg chelatase, archaeal minichromosome maintenance protein MCM from *Sulfolobus solfataricus*, and an archaeal MCM homolog from *Methanopyrus kandleri* (Fig. S3). In all of these proteins, the spatial localization of the all- $\alpha$  subdomain relative to the  $\alpha\beta\alpha$  subdomain is similar to that of RavA and is significantly different

from its typical position found in most other AAA+ members (8, 21).

Fig. 2*C* illustrates the differences between the AAA+ module organization of HslU, a canonical model of the typical AAA+ module fold (15), and RavA AAA+ domain. In HslU, the all- $\alpha$  subdomain is located on “top” of the  $\alpha\beta\alpha$  subdomain. In the all- $\alpha$  subdomain, the Sensor 2 motif (shown in dark blue in Fig. 2*C*), a required motif for nucleotide binding and hydrolysis, is oriented toward the ATP-binding site of the same protomer. In the case of RavA, the all- $\alpha$  subdomain is on the “right” of the  $\alpha\beta\alpha$  subdomain; consequently, the Sensor 2 motif cannot contribute to ATP hydrolysis on the same protomer as in HslU. However, when the X-ray structure of the HslU hexamer is compared to the RavA hexameric model (Fig. 2*D*), then it is clear that HslU and RavA share similar organization of the subdomains in the oligomer although the orientation of the protomers is reversed. In the RavA hexamer, the all- $\alpha$  subdomain of one protomer is located on top of the  $\alpha\beta\alpha$  subdomain of the protomer on its right (Fig. 2*D* and *E*), and the Arg residue of Sensor 2 faces the ATP-binding site of a neighboring protomer (Fig. 2*E* and Fig. S4). In the HslU hexamer, the all- $\alpha$  subdomain of one protomer is located on top of the  $\alpha\beta\alpha$  subdomain of the protomer on its left (Fig. 2*D* and *E*), and the Arg residue of Sensor 2 is facing the ATP-binding site of the same protomer (Fig. 2*E* and Fig. S4). Hence, when viewed from the top, the subunits in RavA are organized clockwise,

whereas the subunits in HslU are organized counterclockwise (Fig. 2D).

It should be noted that, in the RavA structure, the all- $\alpha$  and  $\alpha\beta\alpha$  subdomains from the same monomer make extensive interactions. The buried surface area between these two subdomains is much larger in the case of RavA ( $2,797 \text{ \AA}^2$ ) than for HslU monomer ( $1,084 \text{ \AA}^2$ ) (Fig. 2E). As a result, in the HslU hexamer, the all- $\alpha$  subdomain makes more extensive interactions with the  $\alpha\beta\alpha$  subdomain of the neighboring protomer ( $2,930 \text{ \AA}^2$ ) than in the RavA hexamer ( $754 \text{ \AA}^2$ ).

Even with these major differences in the assembly of the subunits, the overall structures of the RavA and HslU AAA+ hexamers remain similar with a high conservation in the organization of the ATP-binding site. Fig. S4 shows the localization of the nucleotide between two subunits of the RavA and HslU hexamers. In both cases, the nucleotide makes contact with three subdomains. For HslU, the nucleotide is sandwiched between the  $\alpha\beta\alpha$  and the all- $\alpha$  subdomains of the same subunit and faces the  $\alpha\beta\alpha$  subdomain of the left neighboring subunit, whereas the nucleotide in RavA contacts the  $\alpha\beta\alpha$  subdomain of one subunit and faces the all- $\alpha$  and the  $\alpha\beta\alpha$  subdomains of the left neighboring subunit.

**The LARA Domain Mediates RavA-LdcI Interactions.** Previous work in our laboratory has shown that RavA interacts with LdcI, an inducible lysine decarboxylase enzyme, forming an unusual cage-like complex of about 3.3 MDa consisting of two LdcI (81 kDa) decamers and up to five RavA (56 kDa) hexamers (Fig. 3A) (12). We further confirmed this interaction in this study. The pull-down of RavA from an *E. coli* strain in which a Sequential Peptide Affinity (SPA) tag (22) was fused at the 3' end of the endogenous *ravA* gene, also pulled down LdcI as previously observed (12). Analysis of the complex by size exclusion chromatography showed that the majority of RavA was part of a 3.3-MDa complex with LdcI (Fig. S5A), which corresponds to the mass of the complex shown in Fig. 3A. LdcI migrated as a complex with RavA but also as uncomplexed decamers as well. In another experiment, analysis of the interaction between purified RavA and LdcI proteins by sedimentation velocity analytical ultracentrifugation revealed the presence of 0.8-, 2.7-, and 6.0-MDa complexes (Fig. S5B). These complexes would correspond to LdcI decamer alone, the RavA-LdcI cage-like complex of Fig. 3A, and a dimer of the cage-like complex, respectively.

Docking of RavA hexameric model of Fig. 2B and LdcI decameric crystal structure that we recently determined into the EM envelope suggested that the LARA domain of RavA might interact with LdcI (Fig. 3A and Fig. S6A). To determine the validity of the docking model, a RavA construct was made in which the LARA domain was deleted and was termed RavA $\Delta$ LARA (consisting of residues Met1–Ala335 and Leu434–Cys498). An isolated LARA domain construct was also generated (residues Gln329–Glu440). Circular dichroism analysis showed that both proteins have the expected secondary-structure content. Furthermore, RavA $\Delta$ LARA formed a hexameric complex in the presence of ATP (Fig. S6B), and its ATPase activity was similar to that of WT RavA (Fig. S6B, Inset). The interaction of LdcI with RavA and its different constructs was then assessed by surface plasmon resonance (SPR) using the Biacore system. In these experiments, LdcI was immobilized on the chip. The SPR experiments clearly showed that, although WT RavA and LARA domain do interact with LdcI (Fig. 3B), RavA $\Delta$ LARA does not bind to LdcI (Fig. 3C). In the absence of nucleotide, WT RavA bound LdcI with an apparent binding constant of  $0.56 \mu\text{M}$  (Fig. 3B). In the presence of ATP, the binding curve was best fit using two independent binding sites with apparent binding constants of  $0.018 \mu\text{M}$  and  $1.22 \mu\text{M}$  (Fig. 3B). This might indicate that the proper hexamerization of RavA, which is attained in the presence of ATP, allows for two RavA “legs” to bind the LdcI decamer at two different sites as suggested by the docking analysis of Fig. 3A and Fig. S6A. How-

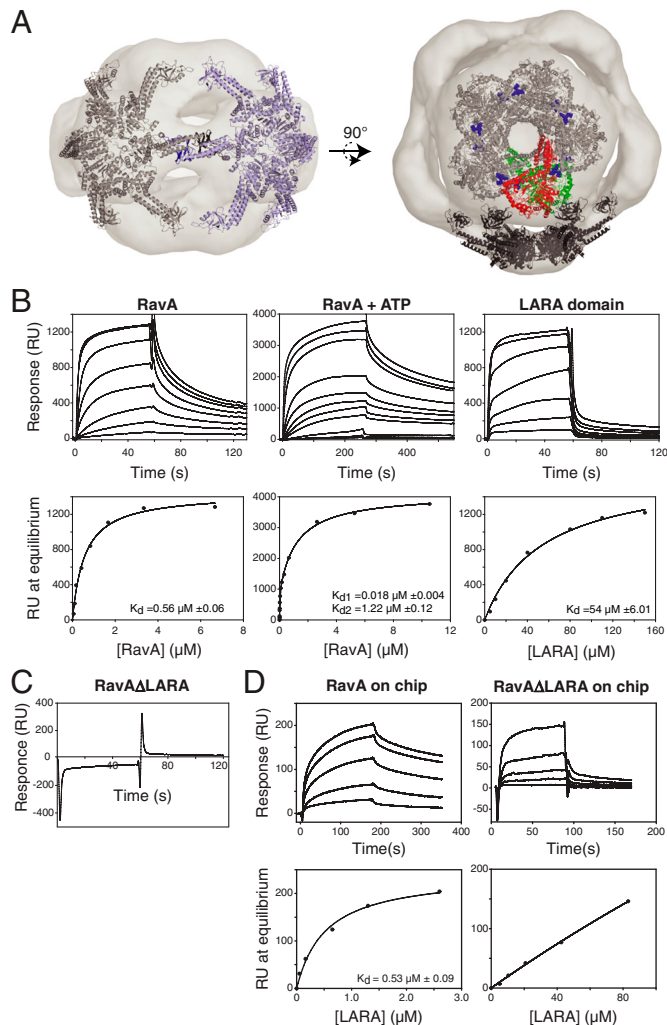


**Fig. 3.** The LARA domain mediates RavA-LdcI and RavA-RavA interactions. (A) Fit of the RavA hexameric model and LdcI decamer into the EM envelope of the LdcI-RavA complex (12) viewed from the side (Left) and the top (Right). One LdcI dimer is colored in red (the upper monomer) and green (the lower monomer). ppGpp bound to LdcI is drawn as blue spheres. (B) Biacore sensorgrams and equilibrium binding curves showing the interaction between LdcI (on chip) and WT RavA in the absence of nucleotide (Left), or WT RavA in the presence of ATP (Middle), or the LARA domain (Right). (C) Biacore sensorgram showing the lack of interaction between LdcI (on chip) and RavA $\Delta$ LARA at  $15 \mu\text{M}$ . (D) Biacore sensorgrams and equilibrium binding curves showing the interaction between WT RavA and LARA domain (Left) and the very weak interaction between RavA $\Delta$ LARA and LARA domain (Right).

ever, it should be noted that, because of the experimental setup, the full complex shown in Fig. 3A, in which RavA hexamers can bridge two LdcI decamers, is unlikely to form under the conditions of the SPR experiments because LdcI is cross-linked to the chip. The isolated LARA domain is also able to bind LdcI albeit with a lower apparent  $K_d$  of  $54 \mu\text{M}$  (Fig. 3B). Hence, these observations strongly suggest that the LARA domain is the RavA domain required for LdcI interaction, hence the acronym LARA: LdcI associating domain of RavA.

Bioinformatic analysis provided further support for the finding that the LARA domain mediates the interaction of RavA with LdcI. In 47 representative bacterial strains that contained RavA based on BLAST searches (23), we asked whether these strains also contain LdcI. As mentioned earlier, the C-terminal fragment of RavA including the triple-helical bundle and LARA domain is not well conserved. Hence, the presence of the LARA domain in RavA across the different strains was assessed using JPred sec-

ondary structure prediction program (24). It was interesting to find that RavA in all strains containing LdcI has a LARA domain, whereas strains that do not have LdcI contain RavA that has or does not have the LARA domain (Fig. S6C). The LARA domain in these strains might have other functions or the domain will eventually degenerate.

**The LARA Domain Mediates RavA-RavA Interactions.** The docking shown in Fig. 3A suggests that the LARA domain might also mediate RavA-RavA interactions within the RavA-LdcI cage-like complex by interacting with the triple-helical domain and/or the LARA domain of the neighboring RavA (Fig. S6D). SPR experiments were carried out in which RavA or RavA $\Delta$ LARA is immobilized on the chip and the LARA domain is titrated. The results indicate that the LARA domain can bind to RavA with an apparent  $K_d$  of about 0.5  $\mu\text{M}$  (Fig. 3D). This interaction is drastically reduced when the binding experiment is performed between RavA $\Delta$ LARA and the LARA domain (Fig. 3D), suggesting that the LARA domain plays an important role in RavA-RavA interactions within the RavA-LdcI cage-like complex.

**RavA Antagonizes the Inhibitory Effect of ppGpp on LdcI Activity.** The LdcI crystal structure revealed the presence of a binding site for the bacterial alarmone guanosine tetraphosphate (ppGpp) at the interface between two protomers in the pentameric ring (Fig. 3A). Biochemical assays showed that ppGpp binding to LdcI results in drastic inhibition of the LdcI activity of approximately 10-fold at pH values greater than 5. The docking shown in Fig. 3A suggests that the LARA domain of RavA might bind at a site in LdcI that could affect ppGpp binding to the decarboxylase.

The activity of the decarboxylase was measured in the presence and absence of RavA and ppGpp using an isothermal titration calorimetry (ITC) approach. Initially, we ensured that the presence of GTP, GDP, ppGpp, and pppGpp does not affect RavA ATPase activity (Fig. 4A). When the RavA-LdcI complex is preformed, LdcI activity is not significantly changed consistent with

our prior observations (12). However, when ppGpp is added to the preformed RavA-LdcI complex, the presence of RavA reduces the inhibitory effect of ppGpp on LdcI by about 40% under the conditions of the experiment (Fig. 4B). Moreover, the RavA- $\Delta$ LARA truncation mutant is not able to reduce the inhibitory effect of ppGpp on LdcI activity, which is consistent with our results showing that the LARA domain is responsible for the RavA-LdcI interaction. When LdcI is preincubated with ppGpp and then RavA is added, RavA is not able to reduce the inhibition of LdcI by the alarmone (Fig. 4C). Hence, RavA either blocks the access to the ppGpp binding site in LdcI or RavA induces a local conformational change in LdcI that reduces its ppGpp binding affinity. Alternatively, ppGpp might cause a conformational change in LdcI to reduce RavA binding to the decarboxylase.

It should be pointed out that the effect of RavA on LdcI inhibition by ppGpp is probably underestimated because these experiments were done at low concentrations of MgCl<sub>2</sub>. Under such conditions, RavA has low ATPase activity; addition of higher concentrations of MgCl<sub>2</sub> lead to the precipitation of ppGpp by Mg<sup>2+</sup>.

To further validate our *in vitro* results and to determine if the modulation of ppGpp binding to LdcI by RavA can be observed *in vivo*, the activity of LdcI was tested in different strains undergoing a stringent response. Four strains were used:  $\Delta$ cadBA, WT + *ravA*, WT + *ravA* $\Delta$ LARA, and WT + *ravA*(K52Q). The last three strains overexpress RavA, RavA $\Delta$ LARA, and RavA(K52Q) proteins by IPTG induction (refer to *Materials and Methods*). RavA(K52Q) is ATPase deficient because the conserved Walker A K52 is mutated to Q (Fig. 1A). Endogenous RavA is expressed at low levels and is induced only in the stationary phase (12). Cells were grown to log phase in defined rich media buffered at pH 5, and, when the OD<sub>600</sub> of each strain was approximately 0.2, proteins were induced with 1 mM IPTG for 1 h. Cells were then shifted to minimal media weakly buffered at pH 5 containing no amino acids to induce ppGpp production, and supplemented with 30 mM lysine to follow the LdcI activity by monitoring pH change of the media; no cell growth occurs during

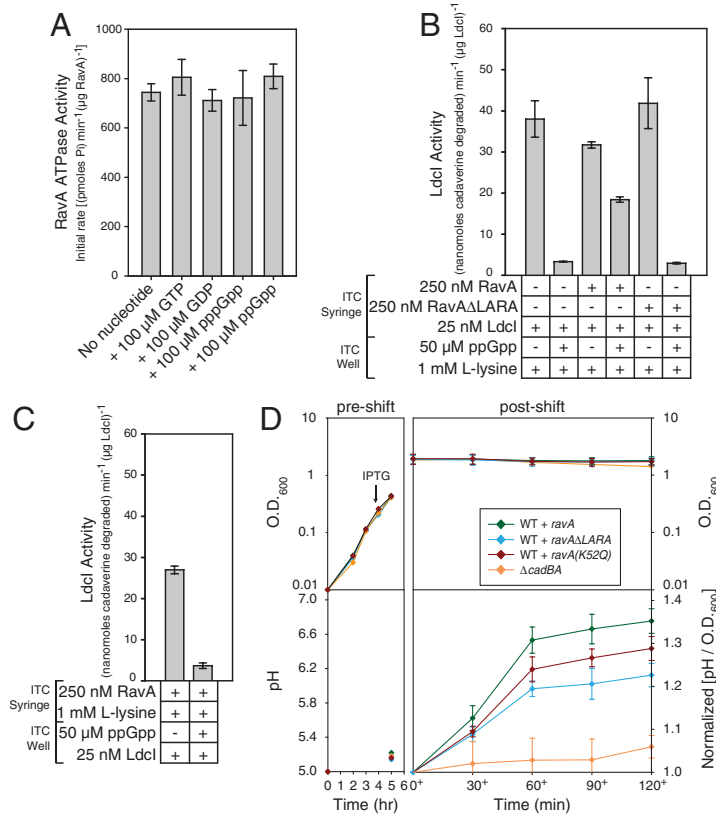


**Fig. 4.** RavA binding to LdcI antagonizes the inhibitory effect of ppGpp on LdcI activity. (A) The ATPase activity of RavA measured by ITC in the presence of different nucleotides. Error bars represent the standard deviation of the average of three experiments. (B) LdcI activity measured by ITC in the presence of RavA or RavA $\Delta$ LARA and/or ppGpp. Note that the concentrations of proteins, substrate, and inhibitor are the final concentrations after mixing. In this panel, the RavA-LdcI complex is preformed in the syringe before adding ppGpp. (C) LdcI activity measured by ITC. In this experiment, LdcI-ppGpp complex is preformed in the well before adding RavA. (D) The effect of RavA overexpression on LdcI activity in the cell.  $\Delta$ cadBA knockout strains and WT cells overexpressing RavA, RavA $\Delta$ LARA, or RavA(K52Q) were grown to log phase in defined rich media buffered at pH 5. RavA, RavA $\Delta$ LARA, or RavA(K52Q) were induced and cells were then shifted to minimal media weakly buffered at pH 5 containing no amino acids to induce ppGpp production and supplemented with 30 mM lysine. The OD<sub>600</sub> of the cells is shown (Top); the pH of the culture media is shown (Bottom Left). (Bottom Right) The increase in pH/OD<sub>600</sub> normalized to the value at 0+ (right after shift). Each time point is the result of at least three replicates. Error bars represent the standard deviations of the measurements.

this time (Fig. 4D and Fig. S7). Consistent with the in vitro results, WT + *ravA* strain increased the pH of the media at a higher rate than the WT + *ravAΔLARA* strain, whereas no significant pH change was observed for the *ΔcadBA* cells (Fig. 4D). Hence, the formation of the RavA-LdcI complex reduced the inhibitory effect of the alarmone on LdcI, allowing the cells to better respond to low acidity. On the other hand, RavA $\Delta$ LARA cannot form a complex with LdcI (Fig. 3D) and, hence, LdcI should still be inhibited by ppGpp resulting in a lower rate of pH increase, as observed (Fig. 4D). The strain overexpressing RavA(K52Q) mutant increased pH faster than the strain overexpressing RavA $\Delta$ LARA, but not as well as the strain overexpressing WT RavA (Fig. 4D), indicating that the binding of RavA to LdcI is not enough to modulate alarmone binding to the decarboxylase, but that the ATPase activity of RavA is also needed.

## Discussion

The organization of the AAA+ module of RavA as revealed by the X-ray structure of the protein (Figs. 1B and 2C) explicitly demonstrates that the protein is closely related to the family of Mg chelatases. We had previously found that RavA and LdcI interact tightly to form an unusual cage-like structure (12). Having the X-ray structure and the EM reconstruction of RavA (this study), as well as the X-ray structure of LdcI and the negative staining EM reconstruction of the RavA-LdcI complex (12), allowed us to gain important insights into the design principles of this cage that is formed by the interaction of a fivefold symmetric oligomer of LdcI with a sixfold symmetric oligomer of RavA (Fig. 3A). The RavA hexamer displays six “legs,” which are spanning the triple-helical domain and the LARA domain. Two of the legs interact with an LdcI dimer at the top of the complex, and two other legs show the same set of interactions with an LdcI dimer at the bottom of the complex. These interactions seem to be mainly mediated by the LARA domain. The two remaining legs of RavA are interacting with a neighboring RavA leg on the left and on the right (Fig. 3A and Fig. S6A). The RavA-RavA leg-leg interactions seem to involve the triple-helical domain, as well as the LARA domain (Fig. 3A). Hence, the construction of the RavA leg makes all these interactions possible. The LARA domain exhibits a unique fold and, based on the bioinformatic analysis of Fig. S6C, seems to be optimally evolved to mediate the interaction of RavA with LdcI.

- Kunau WH, et al. (1993) Two complementary approaches to study peroxisome biogenesis in *Saccharomyces cerevisiae*: Forward and reversed genetics. *Biochimie* 75:209–224.
- Conflanieri F, Duguet M (1995) A 200-amino acid ATPase module in search of a basic function. *Bioessays* 17:639–650.
- Ogura T, Wilkinson AJ (2001) AAA+ superfamily ATPases: Common structure—diverse function. *Genes Cells* 6:575–597.
- Leipe DD, Koonin EV, Aravind L (2003) Evolution and classification of P-loop kinases and related proteins. *J Mol Biol* 333:781–815.
- Ammelburg M, Frickey T, Lupas AN (2006) Classification of AAA+ proteins. *J Struct Biol* 156(1):2–11.
- Snider J, Thibault G, Houry WA (2008) The AAA+ superfamily of functionally diverse proteins. *Genome Biol* 9:216.
- Neuwald AF, Aravind L, Spouge JL, Koonin EV (1999) AAA+: A class of chaperone-like ATPases associated with the assembly, operation, and disassembly of protein complexes. *Genome Res* 9:27–43.
- Iyer LM, Leipe DD, Koonin EV, Aravind L (2004) Evolutionary history and higher order classification of AAA+ ATPases. *J Struct Biol* 146:11–31.
- Ogura T, Whiteheart SW, Wilkinson AJ (2004) Conserved arginine residues implicated in ATP hydrolysis, nucleotide-sensing, and inter-subunit interactions in AAA and AAA+ ATPases. *J Struct Biol* 146:106–112.
- Hanson PI, Whiteheart SW (2005) AAA+ proteins: Have engine, will work. *Nat Rev Mol Cell Biol* 6:519–529.
- Snider J, Houry WA (2006) MoxR AAA+ ATPases: A novel family of molecular chaperones? *J Struct Biol* 156:200–209.
- Snider J, et al. (2006) Formation of a distinctive complex between the inducible bacterial lysine decarboxylase and a novel AAA+ ATPase. *J Biol Chem* 281:1532–1546.
- Krissinel E, Henrick K (2004) Secondary-structure matching (SSM), a new tool for fast protein structure alignment in three dimensions. *Acta Crystallogr D* 60:2256–2268.
- Holm L, Kaariainen S, Rosenstrom P, Schenkel A (2008) Searching protein structure databases with DALIv3. *Bioinformatics* 24:2780–2781.
- Bochtler M, et al. (2000) The structures of HsIU and the ATP-dependent protease HsIU-HsIV. *Nature* 403:800–805.
- Fodje MN, et al. (2001) Interplay between an AAA module and an integrin I domain may regulate the function of magnesium chelatase. *J Mol Biol* 311:111–122.
- Han YW, et al. (2001) A unique beta-hairpin protruding from AAA+ ATPase domain of RuvB motor protein is involved in the interaction with RuvA DNA recognition protein for branch migration of Holliday junctions. *J Biol Chem* 276:35024–35028.
- Lee SY, et al. (2003) Regulation of the transcriptional activator NtrC1: Structural studies of the regulatory and AAA+ ATPase domains. *Genes Dev* 17:2552–2563.
- Shen J, Gai D, Patrick A, Greenleaf WB, Chen XS (2005) The roles of the residues on the channel beta-hairpin and loop structures of simian virus 40 hexameric helicase. *Proc Natl Acad Sci USA* 102:11248–11253.
- Jenkinson ER, Chong JP (2006) Minichromosome maintenance helicase activity is controlled by N- and C-terminal motifs and requires the ATPase domain helix-2 insert. *Proc Natl Acad Sci USA* 103:7613–7618.
- Erzberger JP, Berger JM (2006) Evolutionary relationships and structural mechanisms of AAA+ proteins. *Annu Rev Biophys Biomol Struct* 35:93–114.
- Babu M, et al. (2009) Sequential peptide affinity purification system for the systematic isolation and identification of protein complexes from *Escherichia coli*. *Methods Mol Biol* 564:373–400.
- Altschul SF, et al. (1997) Gapped BLAST and PSI-BLAST: A new generation of protein database search programs. *Nucleic Acids Res* 25:3389–3402.
- Cole C, Barber JD, Barton GJ (2008) The Jpred 3 secondary structure prediction server. *Nucleic Acids Res* 36:W197–201.
- Bond CS (2003) TopDraw: A sketchpad for protein structure topology cartoons. *Bioinformatics* 19:311–312.
- Rocchia W, et al. (2002) Rapid grid-based construction of the molecular surface and the use of induced surface charge to calculate reaction field energies: Applications to the molecular systems and geometric objects. *J Comput Chem* 23:128–137.

The RavA-LdcI cage-like structure might have multiple functions in the cell yet to be elucidated; however, one consequence we found here for the formation of the RavA-LdcI complex is the reduction of the inhibitory effect of ppGpp on LdcI activity. When cells are undergoing acid stress and LdcI is induced to about 2,000 decamers per cell, nutrient limitation will result in the production of the alarmone. Because we estimate that there are about 50–100 RavA hexamers per cell in the stationary phase (12), only a small population of LdcI molecules is expected to be in complex with RavA. This population of LdcI will not be strongly inhibited by ppGpp, allowing the cells to continue to respond to acid stress at the risk of depleting lysine amounts. It is interesting to note that RavA and ppGpp have similar binding constants to LdcI:  $K_d$  of 0.02–1  $\mu\text{M}$  for RavA-LdcI interaction (Fig. 3B) and  $K_d$  of 0.01–0.7  $\mu\text{M}$  for LdcI-ppGpp interaction. The binding of RavA to apo-LdcI does not affect LdcI activity to any significant extent (Fig. 4B and ref. 12). Hence, there is a fine-tuning of LdcI activity by ppGpp and RavA, which is required for the cells to respond to acid stress, as well as to prevent the depletion of their amino acids. This fine-tuning probably involves other factors and proteins and also occurs for other amino acid decarboxylases involved in the bacterial acid stress response.

## Materials and Methods

Details of cloning, protein expression and purification, RavA ATPase assay, SPR measurements, LdcI enzyme kinetics measurements using ITC, sedimentation velocity analytical ultracentrifugation, pull-down experiments, media shift assays, X-ray crystallography, and electron microscopy are provided in *SI Text*.

**ACKNOWLEDGMENTS.** We thank Dr. Elisabeth Tillier (University of Toronto) for her help with the bioinformatic analysis shown in Fig. S6C. We also thank several members of UVHC: Dr. Rob Ruigrok for his support, Dr. Hassan Belrhali for help with data collection and phasing, Dr. Monika Spano, Dr. Nicolas Tarbouriech, and Dr. Thibaut Crépin for help with protein crystallization. M.E.B. is the recipient of a fellowship from the Canadian Institutes of Health Research (CIHR) Strategic Training Program in Protein Folding and Interaction Dynamics: Principles and Diseases. U.K. is the recipient of a National Sciences and Engineering Research Council of Canada (NSERC) Postgraduate Scholarship, a Canadian Institutes of Health Research Strategic Training Program in the Structural Biology of Membrane Proteins Linked to Disease, and a University of Toronto Open Fellowship. B.Z. is the recipient of NSERC Alexander Graham Bell Canada Graduate Scholarship. M.Y. is the recipient of Life Sciences Award from the University of Toronto. This work was supported by a grant from CIHR (MOP-67210) (to W.A.H.).